Iranian Journal of Materials Forming

Research Article

A Hybrid Method of NSGA-II and TOPSIS to Optimize the Performance of Friction Stir Extrusion

M. Akbari[1], P. Asadi[2*] and H. Rahimi Asiabaraki[1]

[1] Department of Mechanical Engineering, Technical and Vocational University (TVU), Tehran, Iran
[2] Advanced Materials Processing and Modeling Lab., Department of Mechanical Engineering, Faculty of Engineering, Imam Khomeini International University, Qazvin, Iran

ARTICLE INFO

ABSTRACT

This study investigates the effect of friction stir back extrusion (FSBE) input parameters such as traverse speed, rotational speed, and wire diameter on the mechanical and microstructural properties of the produced wire. Numerous experiments were performed with different input parameters, and the grain size, hardness, and ultimate pressure strength (UPS) of each of the produced wires were investigated. In addition, to better understand the effect of input parameters, the process was simulated using the finite element method (FEM) model, and the temperature, material flow, and strain distributions in the wires were investigated. Then, using the artificial neural network (ANN), a relationship was obtained between the input parameters of the process, such as traverse speed, rotational speed, and wire diameter, with the mechanical and microstructural properties of the produced wires. This relationship was then used in a hybrid multi-objective optimization to find the optimal process parameters. Due to the higher importance of UPS in comparison to the grain size and microhardness, the weighting of 0.6, 0.2, and 0.2 were used in the TOPSIS model, and the optimum input parameters were achieved as 6 mm, 36.35 mm/min, and 456 rpm, for the traverse speed, rotational speed, and wire diameter, respectively.

© Shiraz University, Shiraz, Iran, 2021

1. Introduction

Brasses (Cu–Zn alloys) comprise of 5 to 45 percent zinc for increased hardness and mechanical resistance, while the rest consists of copper for improved corrosion resistance in various media [1]. As a result, the physical and mechanical properties of these alloys vary depending on their Zn content. They may also contain trace amounts of lead, iron, and other metals. Brasses also exhibit strong electrical and thermal conductivities, as well as great malleability, corrosion resistance, a good balance of strength and ductility, good castability and formability, and excellent machinability [2]. Brass has been used in various fields, including plumbing fixtures and fittings, low-pressure valves, counters and taps, gears, bearings, decorative hardware, architectural frames, musical instruments, germicidal and anti-microbial devices, and architectural frames, due to its excellent and unique properties [3, 4].

Due to limited resources, excessive energy use, and

environmental damage, metal recycling has been a hot concern. Deferent metallic alloys are widely employed in manufacturing practically all types of industrial products. As a result, most waste materials in industrial businesses are metal chips produced during machining. Additionally, shops generate a large number of metal scrap pieces each year, which are then chopped up into chips using shredders. Even though these wastes are generally contaminated with oils and cutting fluids, washing them is much cheaper than mining them. Metal chips are usually re-casted for recycling. Therefore, some companies are required to collect the chips and transport them to the casting shops, where they will be subjected to recasting, rolling, extruding, and other operations to generate the final/useable metal product. The new recycling procedure, Friction Stir Back Extrusion (FSBE), enables workshops to recycle the metal chips straight into extruded products rather than selling them to chip collectors.

Friction-based procedures, such as friction welding, have already proven their capacity to combine and create solid-state materials, resulting in products with desired mechanical properties [5]. With the purpose of processing and recycling chips to produce bulk material, new friction stirring concept was recently developed. As a solid-state recycling technique, the FSBE generates frictional heat to soften the recycling chips. The chips are then combined and pressed into a channel to develop an integrated product such as a wire or tube by exerting adequate pressure called a forging force [6-8].

In each production process, varying the input parameters such as process parameters, tool, and mold sizes, material type, etc., will influence outputs such as mechanical properties. To find the effect of these influencing parameters needs to perform several experiments. However, finding a proper relationship between process inputs and outputs can drastically reduce the cost of experiments along with saving time. In the FSBE process, it is tough to derive these correlations using mathematical equations due to the nonlinear nature of this process. Artificial neural networks (ANN) are one of the most effective solutions to this challenge. Artificial neural networks, which are based on brain neural networks, can extract the relationships between the inputs and outputs of complex processes. So far, this method has been used by researchers in manufacturing processes to model the process. Shojaeefard et al. [9] used the ANN model to establish the correlation between the friction stir welding (FSW) parameters, including traverse and rotational speed, and heat-affected zone (HAZ) width, peak temperature, and axial force values. Their model was able to correctly determine the relationship between input and output parameters in the FSW process. In another study, the relationship between the friction stir process (FSP) parameters and mechanical and microstructural properties of the fabricated composites were determined using ANN [10].

In the present work, the quality of FSBE wires, which were produced by different process parameters, is determined by several factors, including grain size, microhardness, and ultimate pressure strength (UPS). The aim is to optimize the plunging (traverse) speed, rotational speed, and wire diameter; therefore, a multi-objective optimization method must be utilized to account for all of these qualities simultaneously. The non-dominated sorting genetic algorithm-II (NSGA-II), due to its excellent skills in discovering optimal solutions [9-11], is employed to optimize the grain size, microhardness, and UPS of the produced wires and find the optimum process parameters.

2. Experimental Procedure

Brass chips were machined from a CuZn39Pb2Sn brass shaft with the chemical composition stated in Table 1. Before applying the FSBE procedure, these brass chips were packed in a matrix and crushed under 500 kgf

Table 1. Chemical composition of brass

Element	Cu	Zn	Pb	Sn	Fe	Ni	Al	Mn	Si	S	P
wt.%	58.9	37.39	2.14	0.60	0.51	0.43	0.007	0.004	0.003	0.003	0.003

(Fig. 1). The matrix was fabricated from H13 hot-working steel and heat-treated to a hardness of 52 RC. Three Chrome-Nickel steel tools with the dimensions shown in Fig. 2 were made with wire sizing holes of 6, 7, and 8 mm, which were heat-treated to a hardness of 58 RC. Along with the tool dimensions, Fig. 2 shows an image of the manufactured FSBE tool with a 60° conical cut applied to the tool head as the material entrance, allowing the softened material to flow easily toward the cylindrical hole at the tool center. The rotational and traverse speeds were changed from 310 to 800 rpm and from 25 to 40 mm/min, respectively.

The wires are cut perpendicular to the wire axis and polished using a conventional process, then polished and

Fig. 1. Brass chips employed in this investigation to make brass wire.

Fig. 2. The FSBE tool used in this investigation.

etched for microstructural investigations using the optical microscope (OM). The metallographic samples are etched for 20 seconds with a solution of 5 g Fe_3Cl, 30 mL HCl, and 100 mL ethanol, then washed with distilled water and dried.

Using a Vickers microhardness testing machine, the microhardness of the specimens was measured at two places in the wire cross-section (at the center and periphery) by applying a load of 200 g for 15 seconds. The standard pressure test was performed at ambient temperature with a strain rate of 10^{-3} s^{-1} using Cometech universal tensile/pressure test equipment. The pressure test specimens were 12 mm long. A thin film of 1040 oil lubricant was used on both sides of the pressure test samples.

3. Simulation Details

In order to study the process parameters in more depth, it seems necessary to know the temperature distribution in the wires during the process. It is complicated and even impossible to obtain the temperature distribution by using experimental methods due to the large deformation of the material and the very high force applied. For this purpose, the FSBE process was modeled using Deform-3DTM software, which is one of the best software for modeling processes with high plastic deformation. In this study, an arbitrary Lagrangian-Eulerian formulation was selected for the numerical simulation of the process [12]. The FSBE tool was considered as a rigid body and meshed with 32000 tetrahedral elements. Moreover, the workpiece was partitioned into two zones and meshed with different tetrahedral element sizes. Smaller meshes in the mean length of 0.8 mm are used on top of the workpiece, which is subject to excessive plastic deformation (Fig. 3).

The flow stress of Brass aluminum alloy is given as a function of strain rate, plastic strain, and temperature:

$$\bar{\sigma} = \bar{\sigma}(\bar{\varepsilon}, \dot{\bar{\varepsilon}}, T) \tag{1}$$

where $\bar{\sigma}$ represents the flow stress, $\bar{\varepsilon}$ represents the plastic strain, $\dot{\bar{\varepsilon}}$ represents the strain rate, and T is the
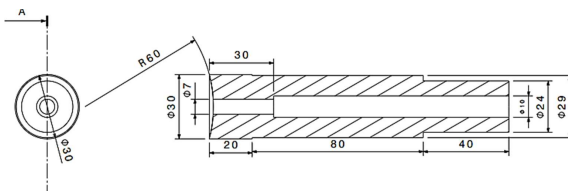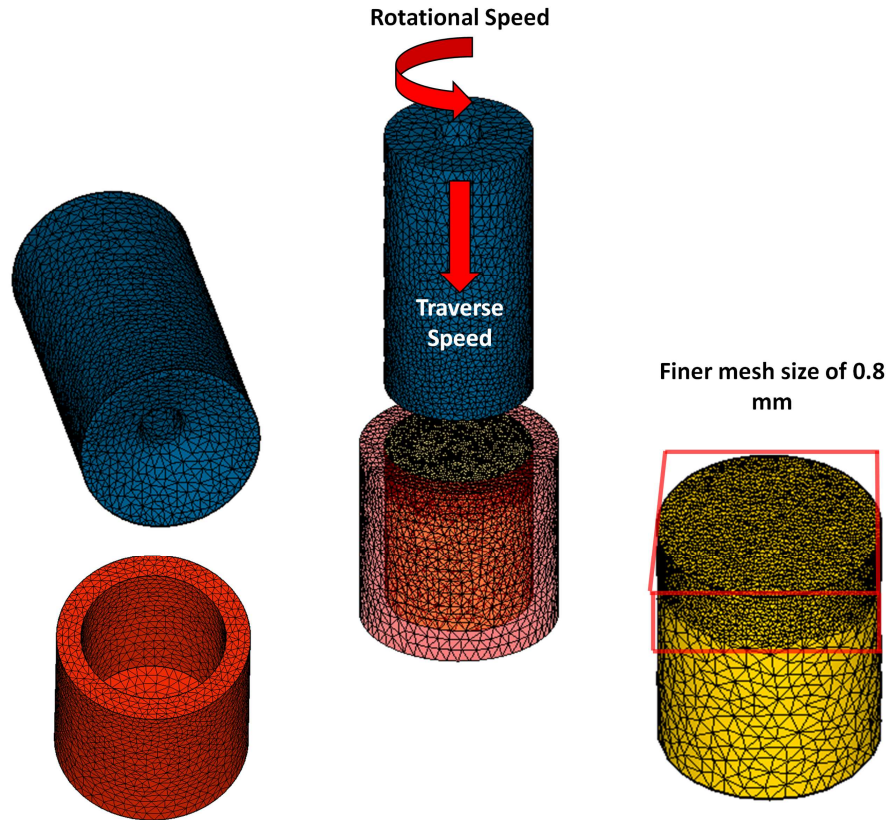
Fig. 3. Illustration of the workpiece and the FSP tool.

temperature. The material flow model used is from the laboratory results available in the DEFORM software library.

Constant shear friction is utilized to model friction between tool and workpiece in this study. In the constant shear model, the frictional force could be calculated as follows:

$$f = mk \qquad (2)$$

where *f*, *k,* and m represent the frictional stress at the tool-workpiece interface, the shear yield stress, and the shear friction factor. Based on previous experimental works, a constant friction factor of 0.4 was employed for the tool-workpiece [13]. The thermal properties of the workpiece and tool are summarized in Table 2. Heat transfer coefficients have been selected based on the research of Tutunchilar et al. [14]. It was also assumed that 90% of the friction heat was transferred to the workpiece.

Table 2. Thermal characteristics of the workpiece, tool, and matrix

Property	Brass	Tool	Matrix
Heat capacity (N/mm² °C)	3.105	3.3	3.3
Emissivity	0.7	0.7	0.7
Conductivity (N/s °C)	122	24.5	24.5
Heat transfer coefficient between tool and billet (N/°C s mm)	11	11	-
Heat transfer coefficient between matrix and billet (N/°C s mm)	11	-	11

The simulation and experimental thermal history curves are compared to verify model accuracy (Fig. 4). Temperatures are measured on the matrix body at 3 mm from the inside of the cylindrical surface and 10 mm from the top surface. The experimental and numerical temperature history that graphs over the process are illustrated in Fig. 4, showing good agreement between them.
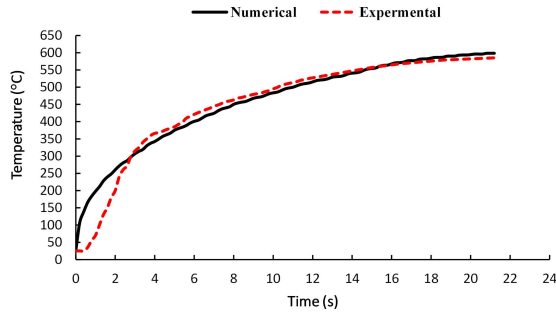
Fig. 4. The experimental and numerical temperature history curves.

4. Results and Discussion

In this study, first, the mechanical and microstructural properties of the produced wires were investigated. Then, using experimental and simulation results, the effect of parameters on the microstructural and mechanical properties of the produced wires is investigated. The process was then modeled using neural networks, and this model was used in a multi-objective optimization algorithm to optimize the process parameters.

4.1. Temperature distribution

Fig. 5 depicts the temperature distribution for extruded workpieces at various tool rotational and traverse speeds. The required heat for material softening in the FSBE, like other friction-stir-based processes, is primarily created by friction at the tool/workpiece interface. The plastic deformation heat is then added to the total generated heat by flowing the material. The generated heat softens the material, which elevates the workpiece temperature to 60-95% of the substance's melting point [15]. Then the axial movement is applied to the tool to deform the workpiece and reduce its diameter from extrusion chamber diameter to the wire diameter.

As shown in Fig. 5, the maximum temperature is reached under the tool shoulder in all specimens, where the tool has the most force and speed. In addition, most plastic deformation occurs in this area, which is another reason for the higher temperature below the tool shoulder. As can be seen in this figure, by increasing the rotational speed of the tool, the heat produced in the sample increases, and, as a result, the temperature of the samples rises as well. By reducing the rotational speed, the generation of both frictional and plastic deformation heat diminishes. As the tool speed increases from 315 to 800 rpm at a constant traverse speed of 31.5 mm/min, the maximum temperature increases from 566 to 646°C.

The tool's traverse speed effects on the heat generated and the resulting wire temperature can be seen in Fig. 6. As the traverse speed of the instrument increases from 25 to 40 mm/min, the maximum temperature changes from 601 to 648°C. Two opposite
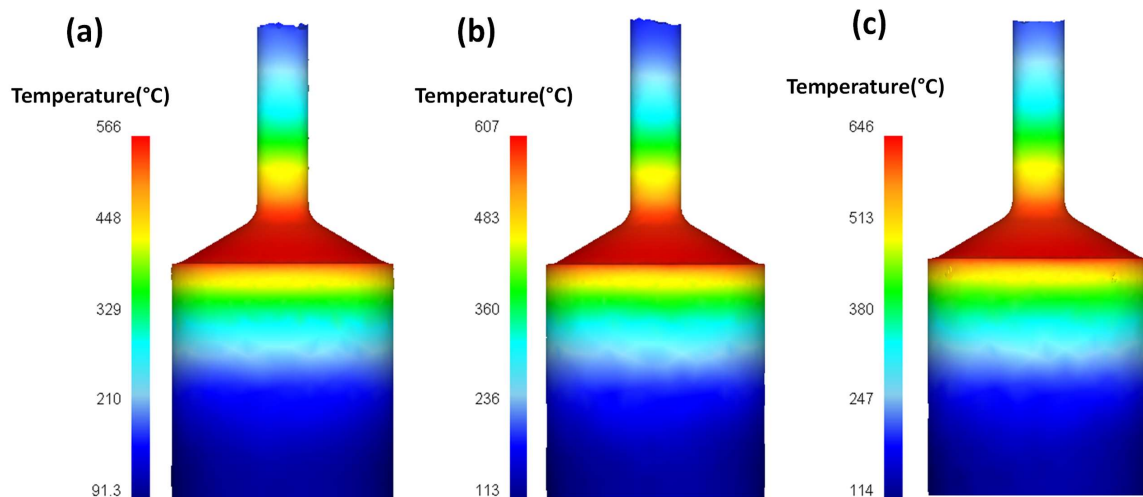

Fig. 5. Temperature distribution during the FSBE process at a traverse speed of 31.5mm and a rotational speed of (a) 315 rpm, (b) 500 rpm, (c) 800 rpm.
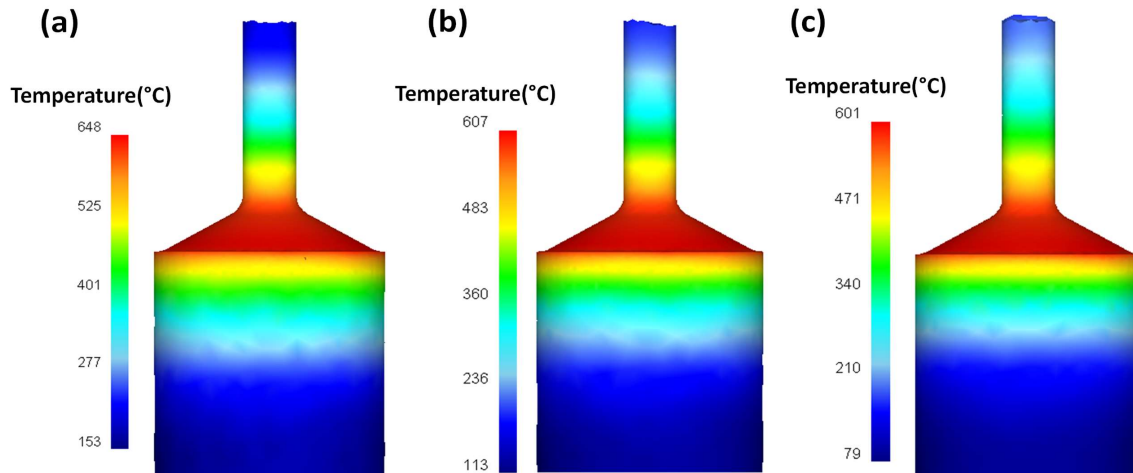
Fig. 6. Temperature distribution during the FSBE process at a rotational speed of 500 rpm and a traverse speed of (a) 25 mm/min, (b) 31.5 mm/min, (c) 40 mm/min.

factors are influential in this increase in temperature. First, by increasing traverse speed of the tool, the force applied to the workpiece increases [16], and as a result, the heat generated due to friction will rise due to the growth in vertical force. On the other hand, increasing the traverse speed reduces the processing time and the time that the workpiece is exposed to heat, thus reducing the workpiece temperature [17].

As shown in Fig. 6, increasing the traverse speed reduces the temperature of the workpiece, indicating that the processing time is the dominant parameter in determining the temperature. It may be determined by comparing the maximum temperature reached in

different process parameters that samples with a greater rotational speed to traverse speed ratio (ω/v) have a higher maximum temperature.

In Fig. 7, the effect of the diameter of the wires on the temperature is specified. As the diameter of the wire increases, more material must enter the tool, and, as a result, more time is required to produce the wire at the same traverse speed. As the processing time increases, the material is heated for a longer time, and, as a result, its temperature rises. However, the effect of changing the wire diameter on temperature is negligible compared to the impact of the previous two variables, traverse speed, and rotational speed.
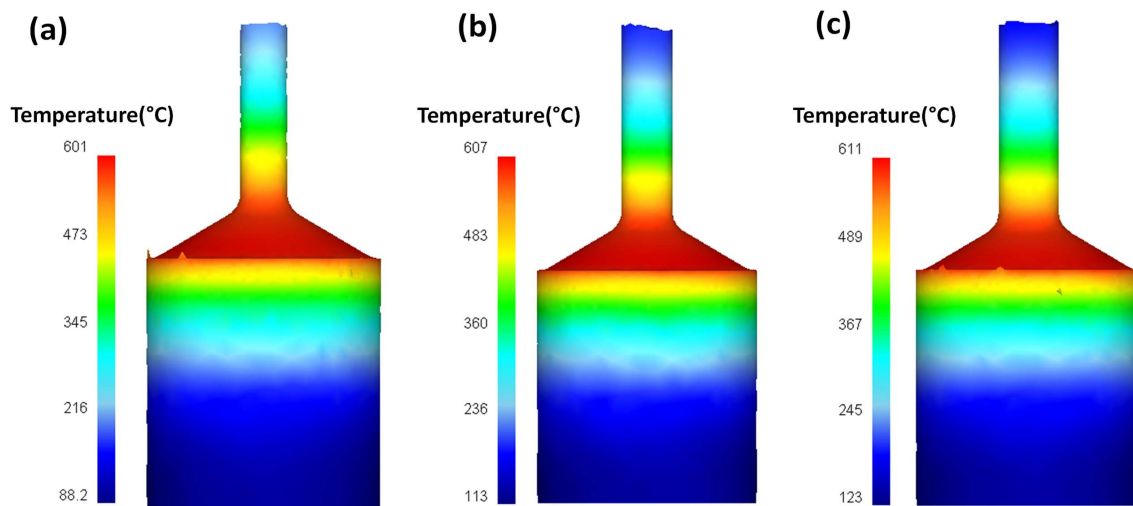

Fig. 7. Temperature distribution during the FSBE process at a rotational speed of 500 rpm and a wire diameter of (a) 6 mm, (b) 7 mm, (c) 8 mm.

4.2. Characteristics of produced wire by FSBE

The cross-section macrograph of the FSBE-produced wire is shown in Fig. 8(a). The FSBE process can produce a defect-free brass wire by recycling brass chips, as demonstrated in this figure. The peripheral and central microstructures of the cross-section of the generated wires by FSBE at different process parameters are shown in Figs. 8(b) and 8(c). The periphery microstructure in both samples is more refined than the center microstructure. The amount of strain and the temperature encountered are related to this differential, which will also affect the microhardness [16].

Due to the increased linear velocity of the tool at the wire perimeter rather than the tool center, the materials at the wire periphery incur more strain (Fig. 9(a)). It is widely known that increasing the strain reduces the grain size in the generated microstructure by increasing the nucleation sites over the recrystallization.

Regarding the experienced temperature over the processing time, it could be declared that the surface of the FSBE tool acts as a heat well and cools the outer surface of the wires that are in contact with the tool, and
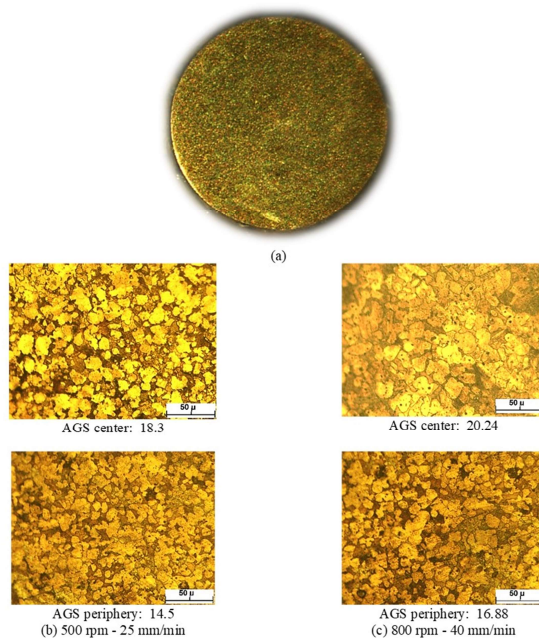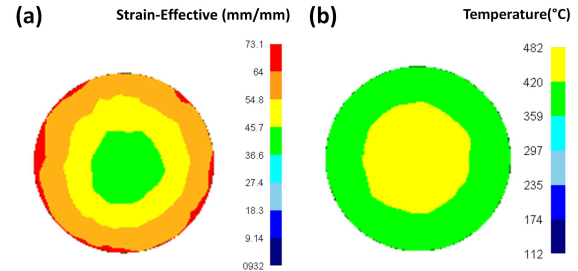
Fig. 9. (a) Strain distribution and (b) temperature distribution on the cross-section of the wires produced at a rotational speed of 500 rpm and a traverse speed of 31.5 mm/min.

as a result, the temperature at the surface of the wires is lower than the center of the wire (Fig. 9(b)). As a result, the lower experienced temperature at the wire periphery reduces the grain growth during the process. Higher strain and lower temperature of the outer surface of the wires is the main reason for the smaller grain size in this area.

In order to better understand the difference between the microstructure in the center and periphery of the wires produced, the material flow in these two areas was modeled. In the original stock, the points are 1 and 3 mm from the center axis (see Fig. 10). From 3D, front, and top views, their routes through the process from initial stock to final wire sample may be seen. As can be observed, from the starting stock to the size channel, where the wire is formed, all points spin around the axis and climb in a virtually helical manner. The path for the point in the center zone, on the other hand, is almost entirely helical and moves practically vertically at a slower rate. The path is a conical helix for the point at the wire's periphery, and it takes an inward spiral movement in addition to upward movement. Therefore, it must follow the longer path with higher speed. As a result, as previously stated, a greater strain is applied to the points near the wire's periphery. The higher the strain, the higher the dislocation density and the more favorable sites for grain nucleation, resulting in a microstructure with more refined grains.

Even though there are visible grain size disparities between the center and periphery of the generated samples, the center values are used to optimize the process parameters.

Fig. 8. (a) Cross-section macro image of the produced brass wire by FSBE. central and peripheral microstructures of the samples produced at (b) a traverse speed of 25 mm/min and a rotational speed of 500 rpm, (c) a traverse speed of 40, and a rotational speed of 800.
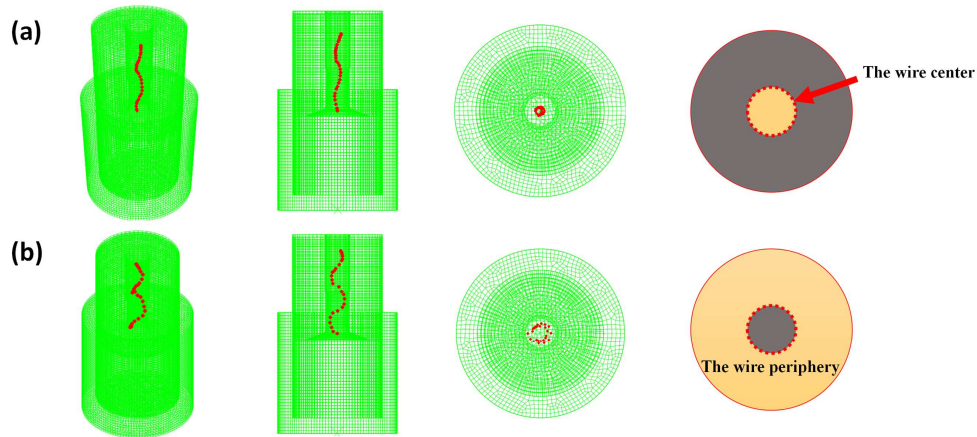
Fig. 10. Material flow behavior in two areas (a) the center and (b) periphery.

Table 3 shows the central microhardness of the manufactured samples. Based on the microstructural data, the microhardness value in the sample perimeter should be larger than that of the sample core. The center microhardness of a sample made with a traverse speed of 25 mm/min and a rotational speed of 500 rpm, as well as a sample made with a traverse speed of 40 mm/min and a rotational speed of 800 rpm, is 121 and 119 HV,

Table 3. The experimental data used in the neural network

	Traverse Speed (mm/min)	Rotational Speed (rpm)	Wire Diameter (mm)	Grain Size (μm)	Hardness (HV)	UPS (MPa)
1	25	315	6	12.1	133	863
2	25	500	6	17	123	888
3	25	800	6	25.7	113	869
4	25	315	7	12.71	131.3	850
5	25	500	7	18.3	121	871
6	25	800	7	28.3	110.4	860
7	25	315	8	13.6	129	820
8	25	500	8	19.8	119	863
9	25	800	8	30.4	106	832
10	31.5	315	6	10.8	136.2	870
11	31.5	500	6	15.05	126	940
12	31.5	800	6	20.1	119	856
13	31.5	315	7	11.91	132.8	839
14	31.5	500	7	16.91	122.5	932
15	31.5	800	7	22.55	116	832
16	31.5	315	8	13.13	130	820
17	31.5	500	8	18.8	120	899
18	31.5	800	8	24.7	114	811
19	40	315	6	9.2	142	650
20	40	500	6	13.1	130	818
21	40	800	6	19	120	831
22	40	315	7	9.59	139	520
23	40	500	7	14.17	128.3	792
24	40	800	7	20.3	119	824
25	40	315	8	10.7	135	706
26	40	500	8	15.8	125	750
27	40	800	8	22.1	116.4	804

respectively, whereas the peripheral microhardness is 129 and 123 HV. The grain size is the leading cause of greater hardness near the sample's periphery (Fig. 7).

Fig. 11 shows the engineering stress-strain pressure test curves for a sample generated at a traverse speed of 25 mm/min and a rotational speed of 500 rpm, as well as a sample produced at a traverse speed of 40 mm/min and a rotational speed of 800 rpm. In section 4.5, the impact of process factors on the UPS of produced samples will be addressed.

4.3. Effect of input parameters on grain size

The influence of process parameters, including traverse speed, rotational speed, and wire diameter, is shown in Figs. 12 and 13. As discussed in the preceding section, raising the tool's rotating speed raises the temperature of the workpiece during the process, hastening grain growth. By reducing processing time and limiting frictional heat generation, the traverse speed has the opposite effect and reduces temperature.

The base part of deformation is generated by rotating speed during the process, and increasing rotational speed promotes deformation. The grain structure that results should be more refined as a result of this. Because more severe recrystallization with a more considerable number of nucleation sites occurs with higher deformation [18, 19]. However, the results showed that the temperature of the workpiece is the dominant parameter in determining the grain size compared to the amount of plastic deformation of materials. As shown in Fig. 12, the grain size increases in the wires produced by increasing the rotational speed or decreasing the traverse speed.

Fig. 13 shows the effect of wire diameter on the grain size of those wires. Two factors affect the change in grain size by changing the diameter of the wires. First, as the diameter of the wire increases, the temperature produced in the wire increases due to the increased processing time, which intensifies grain growth. Furthermore, the larger tool central hole (which creates a larger-diameter wire) minimizes plunging force during the process, resulting in less strain in the processed materials. As a result, the nucleation sites decrease during
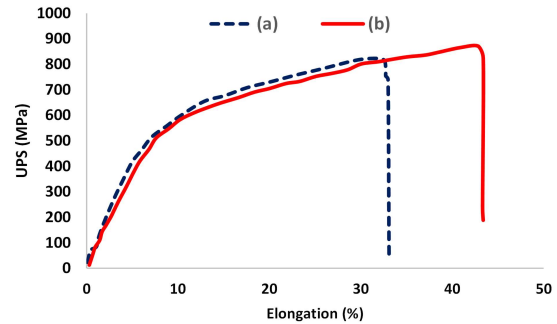

Fig. 11. The engineering stress-strain pressure test curves for samples produced at (a) a traverse speed of 25 mm/min and a rotational speed of 500 rpm, (b) a traverse speed of 40 mm/min, and a rotational speed of 800 rpm.
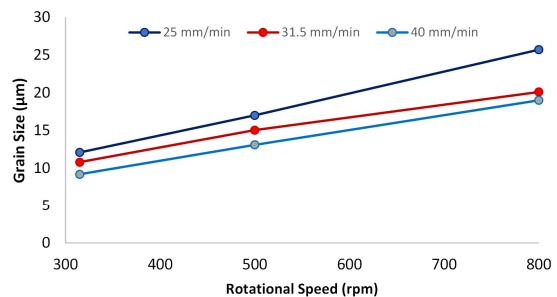

Fig. 12. The effect of rotational and traverse speed on the grain size of the wires.
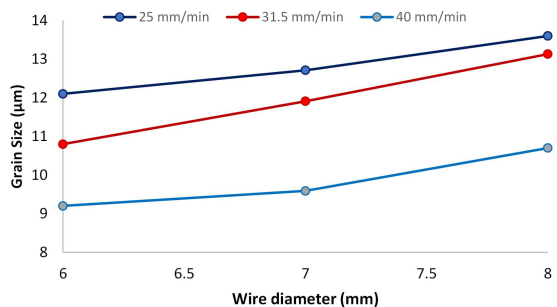

Fig. 13. The effect of wire diameter on the grain size of the wires.

during the recrystallization process, resulting in a coarser microstructure in the generated wire. The smallest grain size is reached when a 6 mm diameter wire is produced, as seen in Fig. 13.

4.4. Microhardness as a function of input parameters

Figs. 14 and 15 illustrate the variation of microhardness versus the different tool traverse and rotational speeds and wire diameter. As it is known, increasing the traverse speed or decreasing the rotational speed and diameter of the produced wires increases the
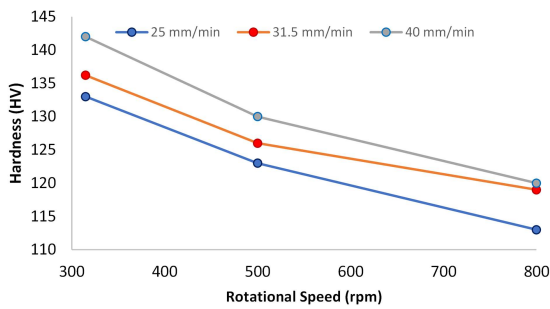
Fig. 14. The effect of rotational and traverse speed on the hardness of the wires.
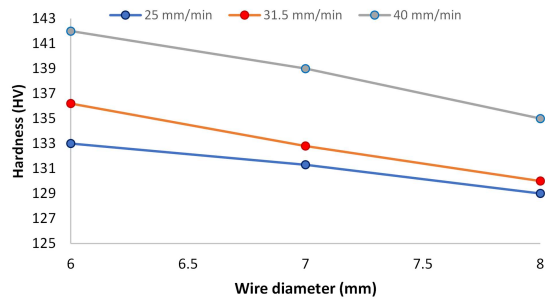

Fig. 16. The effect of rotational and traverse speed on UPS of the wires.

Fig. 15. The effect of wire diameter on the hardness of the wires.
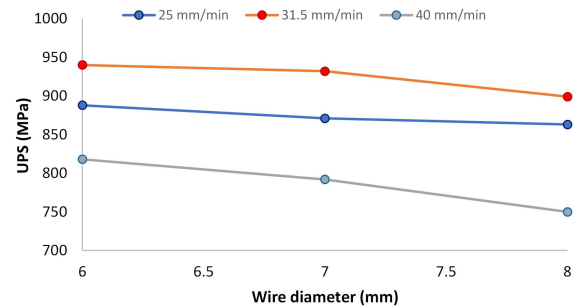
Fig. 17. The effect of wire diameter on UPS of the wires.

hardness of the samples. The effects of the parameters on the hardness are opposite to their impact on the grain size. According to the Hall-Petch relationship, grain size affects the hardness of alloys, and the hardness increases by decreasing the grain size [20, 21].

4.5. Effect of input parameters on UPS

The variation curves of UPS vs. tool rotating speed, traverse speed, and wire diameter are shown in Figs 16 and 17. UPS behaves differently when it comes to the input parameters than it does when it comes to the grain size and hardness of the samples. The UPS of the samples appears to be influenced by a factor other than temperature and strain. Although its microstructure and hardness determine the strength of a material, discontinuities in the macrostructure caused by inadequate material flow during the FSBE process substantially impact the UPS in the samples generated.

Since the temperature and grain size are lowered, and hardness is enhanced. Additionally, by increasing the traverse speed, the UPS should be increased. The traversal speed ranged from 25 to 31.5 mm/min when this
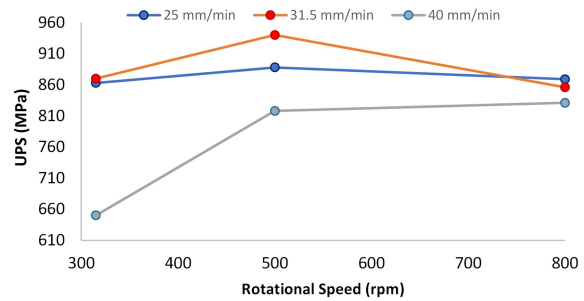
event occurred. To put it another way, a faster traverse speed will result in a higher UPS.

However, the defect that appeared in the center of the produced sample at a traverse speed of 40 mm/min (Fig. 18) demonstrates that insufficient heat generation causes poor formability of the materials in the process, which leads to the production of discontinuity in the sample core. In reality, the poor softening of material due to the lack of heat results in a poor material flow (strain) in the materials under process. The manufactured wire UPS is drastically reduced as a result of this serious flaw.

It should be noticed that the temperature and strain have a bilateral effect on themselves. Lower temperature weakens the material flow and strain. While on the other side, the heat generated from plastic deformation will be lowered in low strains and weak flow of materials, consequently, decreasing the temperature. Therefore, it could be mentioned that the lack of both strain and generated heat leads to the generation of defects.

The influence of rotational speed also exhibits reversal behavior. As mentioned in section 4.4, increasing the rotational speed decreased the microhardness (Fig. 14); hence the wire generated at the
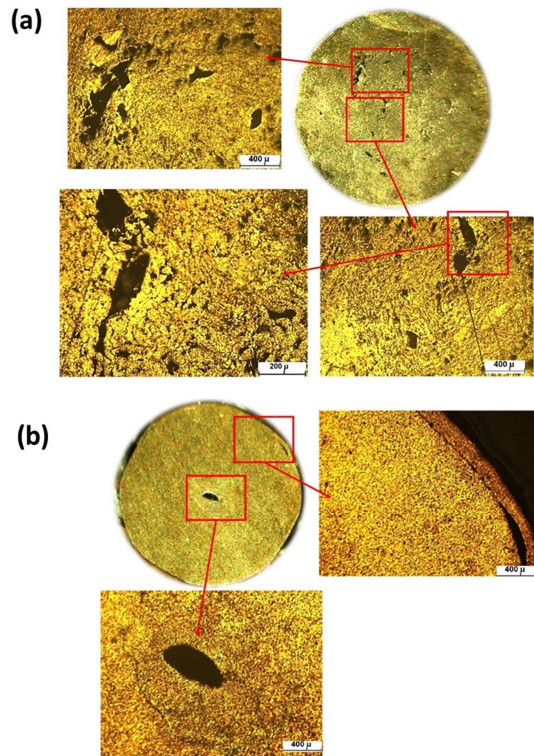
Fig. 18. The defects generated in the cross-section of the wires produced with the traverse and rotational speeds of (a) 40 mm/min and 315 rpm, and (b) 40 mm/min 500 rpm.

higher rotating speed should have a lower UPS. Increase the rotating speed from 500 to 800 rpm to see this behavior, which reduces the UPS. However, the rotating speed of 315 rpm has unexpectedly resulted in the lowest UPS. Similarly, a fault in the cross-section of the wire caused this much lower UPS.

Although the influence of wire diameter variation on the UPS is intangible, it appears that increasing the diameter of the produced sample causes a reduction in strength. In fact, the axial forging force necessary to pass the under-process material over a smaller hole is greater than that required to pass the material over a larger hole. As a result, a smaller tool center hole could generate a stronger material (which produces a smaller wire diameter).

4.6. Modeling using ANN

As it turned out from the experimental results, the input parameters significantly affected the microstructural and mechanical properties of the process. In manufacturing processes, due to the high cost of production, it is impossible to use all input parameters to determine the product's properties. The use of numerical methods to model the relationship between input parameters and output properties of the product makes it possible to determine output properties based on input parameters without performing experimental tests. One of these numerical models is neural networks, which have been widely used in modeling manufacturing processes. This research uses an artificial neural network to obtain a relationship between process inputs such as rotational speed, traverse speed, and wire diameter and output parameters such as UPS, hardness, and grain size.

For this reason, a feed-forward neural network with a back-propagation algorithm was used to predict the required results without performing an experiment. A feed network is a network in which the output of neurons is connected only with the neurons of the next layer [9, 11, 22]. Additionally, the output and input data from the experiment were normalized in the range of 0 to 1 for use in the neural network. Neural network model and multivariate optimization were performed with MATLAB software. In order to develop the neural network model, twenty-seven sets of experimental data obtained using different input parameters were used (Table 3). Moreover, Levenberg-Marquardt (LM) was used as a training algorithm. The LM algorithm is commonly used to tackle nonlinear least squares issues. This approach uses a combination of gradient descent and Gauss-Newton methods [23].

In the development of neural networks, the selection of parameters affecting the network, such as the number of hidden layers and the functions used, play a vital role in the neural network's performance. Several neural networks were examined using different parameters to select the optimal neural network parameters, and the network with the lowest error between the experimental data and the predicted data was established. The developed neural network consists of 3 neurons in the input layer, 10 neurons in the hidden layer, and 3 neurons in the output layer. The Mean Relative Error (MRE) criterion was used to evaluate the performance of each of these networks:

MRE =

$$\frac{1}{P}\sum_{1}^{P}(\frac{|experimental\ value - predicted\ value|}{experimental\ value} \times 100) \quad (3)$$

The minimum MRE in the network with ten hidden layers as well as Logsig activation functions in both layers is achieved (Fig. 19) [9, 11, 22]. In the development of neural networks, some data are used to train neural networks and others to test the function of neural networks. In this study, about 20% of the experimental data were used for testing and the rest for neural network training. The neural network error during the training and testing stage for the various parameters is given in Table 4. As can be seen, the neural network has been able to predict the results in both stages.
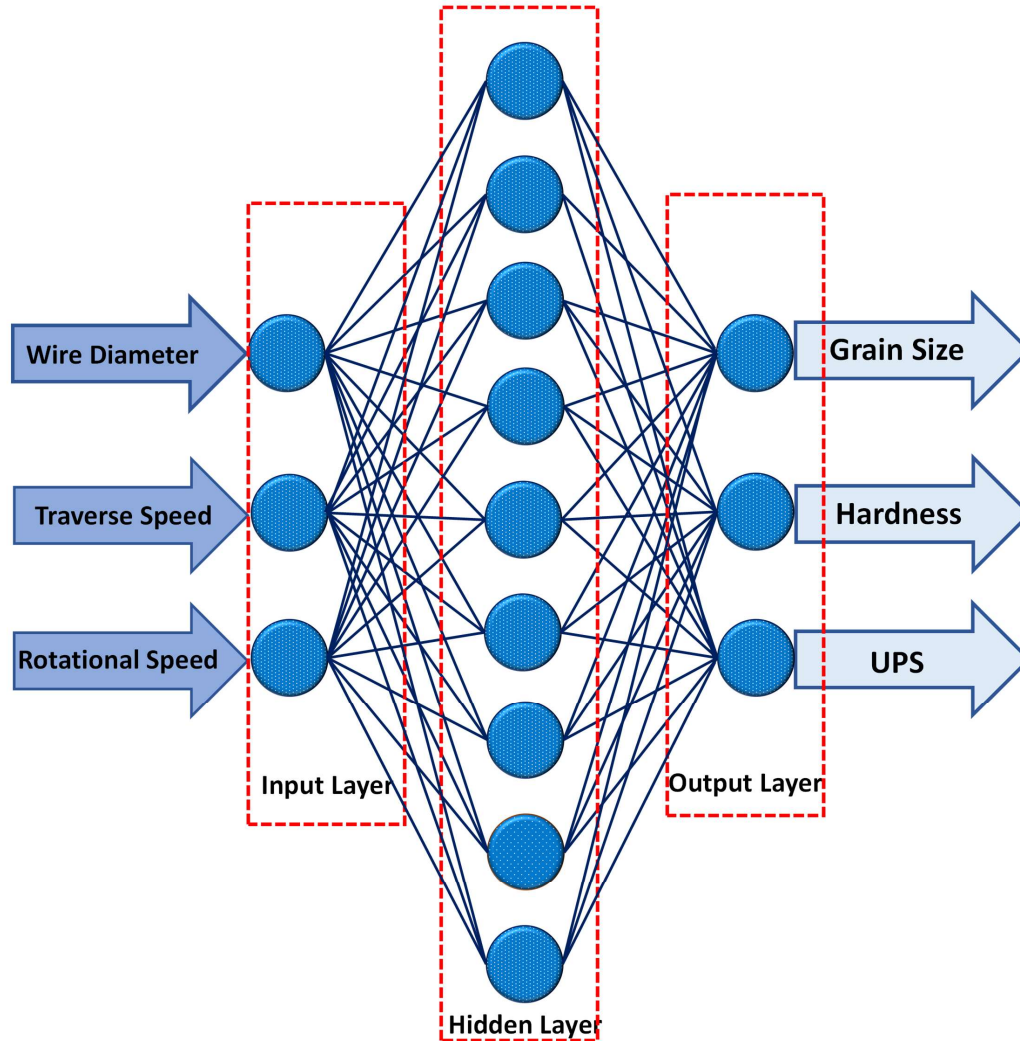

Fig. 19. Three-layer neural network used in this study.

Table 4. Neural network errors in two stages of training and testing

	MRE	
	Train Stage (%)	**Test Stage (%)**
Grain size	1.765130255	7.488925
Hardness	0.774006694	1.544752
UPS	0.84007045	8.454584

Eqs. (4)-(6) were obtained from ANN based on the input parameters of traverse speed, rotational speed, and wire diameter to determine the grain size, hardness, and UPS

as outputs of the model. Similarly, using these equations (Eqs. (4)-(6)), grain size, hardness and UPS may be calculated as:

$$Grain\ Size\ = \left(\frac{40}{1 + e^{-(-1.77 \times F_1 - 0.036 \times F_2 + 7.1 \times F_3 + 1.8 \times F_4 + 1.1 \times F_5 - 6.07 \times F_6 - 0.6 \times F_7 - 4.193 \times F_8 - 0.57 \times F_9 + 1.3 \times F_{10} + 3.38)}}\right) \quad (4)$$

$$Hardness\ = \left(\frac{160}{1 + e^{-(2.94 \times F_1 + 0.16 \times F_2 - 2.27 \times F_3 - 2.2 \times F_4 - 0.91 \times F_5 + 1.95 \times F_6 + 0.76 \times F_7 + 2.14 \times F_8 + 0.61 \times F_9 - 1.83 \times F_{10} + 1.42)}}\right) \quad (5)$$

$$UPS = \left(\frac{1000}{1 + e^{-(1.46 \times F_1 + 10.12 \times F_2 + 2.3 \times F_3 + 9.5 \times F_4 + 5.6 \times F_5 + 4.8 \times F_6 + 18.5 \times F_7 + 9.1 \times F_8 - 4.64 \times F_9 + 8.69 \times F_{10} - 21.63)}}\right) \quad (6)$$

where F_i (i = 1, 2, 3, ..., 10) are the weights, can be calculated using:

$$F_i = \frac{1}{1 + exp^{-U_i}} \quad (7)$$

where $i=1,....,10$ and U_i can be determined by Eq. (8):

$$U_i = C_{1i} \times T + C_{2i} \times R + C_{3i} \times d + C_{4i} \quad (8)$$

Constants, C_{ji}, in Eq. (8), are given in Table 5 LM algorithm, and T, R, and d, are traverse speed, rotational speeds, and wire diameter, respectively. T, R, and d values are normalized by being divided by 50, 1000, and 10.

Table 5. The weights and biases between input and hidden layers for Eq. (8)

$U_i = C_{1i} \times T + C_{2i} \times R + C_{3i} \times d + C_{4i}$			
i	C_{1i}	C_{2i}	C_{3i}	C_{4i}
1	4.8668	10.27	-51.36	15.86
2	-32.4117	-1.6	41.31	2.507
3	16.82	12.71	-4.34	-40.91
4	12.1456	30.029	-45.93	13.561
5	-0.46	17.51	-46.41	19.70
6	2.37	-1.91	-5.09	5.18
7	6.65	1.28	-37.38	16.46
8	31.99	-5.6	-18.631	-23.38
9	13.0316	22.79	-76.008	30.38
10	-21.21	-38.43	66.303	-19.60

4.7. Analysis of variance (ANOVA)

Controlling the input parameters to produce quality samples requires understanding the impact of each input parameter on the performance of the produced samples. The relevance of input parameters can be calculated using a variety of ways. The ANOVA method, a statistical tool for testing the differences between two or

more means, is being considered by researchers as one of these methods for analyzing sensitivity [24]. In this study, this analysis was used to investigate the importance of the parameters. Sensitivity analysis of process outputs, including grain size, hardness, and UPS, is shown in Table 6. As shown in this table, rotational speed is the dominant parameter in determining the grain size and hardness of the samples. In the production of wires, the deviation from the optimal rotational speed creates the most significant deviation in the properties of the wires produced from the desired value, and precise control of this parameter seems to be critical compared to other parameters. In addition, as shown in Table 6, the most critical parameter on the UPS of wires produced is traverse speed, with a contribution of 65.29%. As discussed before, increasing the traverse speed causes defects such as discontinuities in the wires, which cause a sharp drop in UPS.

4.8. Multi-objective optimization

In this research, hybrid optimization has been used to optimize the process parameters. This optimization consists of two parts. First, the Pareto front is obtained using the NSGA-II method. Then, using the TOPSIS method and weighting the objectives based on their importance, the optimal parameter is selected from the Pareto solutions.

Multi-objective optimization, which is also called multi-criteria optimization, is used in processes where the output is more than one in order to optimize all objectives simultaneously. The objectives in these processes are often in conflict with each other and improving one objective will worsen another. For this

Table 6. Analysis of variance of objectives

Grain size					
Source	**Sum Sq.**	**d.f.**	**Mean Sq.**	**F**	**Contribution (%)**
Traverse Speed	107.6031	2	53.8016	33.6584	13.12511016
Rotational Speed	671.7368	2	335.8684	210.1199	81.93636164
Wire diameter	40.4874	2	20.2437	12.6645	4.938528202
Error	31.9692	20	1.5985		
Total	851.7965	26			
Hardness					
Source	**Sum Sq.**	**d.f.**	**Mean Sq.**	**F**	**Contribution (%)**
Traverse Speed	265.5141	2	132.757	83.5573	12.72033718
Rotational Speed	1694.574	2	847.287	533.2824	81.18419266
Wire diameter	127.2319	2	63.6159	40.0399	6.095470159
Error	31.7763	20	1.5888		
Total	2119.096	26			
UPS					
Source	**Sum Sq.**	**d.f.**	**Mean Sq.**	**F**	**Contribution (%)**
Traverse Speed	84005.41	2	42002.7	13.4021	65.29796297
Rotational Speed	39131.19	2	19565.59	6.2429	30.41677446
Wire diameter	5512.963	2	2756.482	0.87953	4.285262561
Error	62680.96	20	3134.048		
Total	191330.5	26			

reason, no one answer optimizes all objectives simultaneously. There is a set of answers to these problems as the optimal answer known as Pareto front or Pareto optimal solutions. The concept of Pareto front stands for a set of solutions that are non-dominated by each other but superior to the rest of the solutions in the search space. The answers in the Pareto front cannot be optimized with respect to an objective unless at least another objective gets worse.

So far, various algorithms have been proposed to solve multi-objective optimization problems. The most widely used multi-objective optimization algorithms based on evolutionary algorithms are presented. Among the meta-heuristic algorithms for multi-objective optimization, the NSGA-II algorithm, which is a modified version of the NSGA algorithm, has received more attention due to its excellent performance in determining optimal solutions. Therefore, in this study, the NSGA-II algorithm is used to optimize process parameters.

In order to determine the optimal values of the process, such as hardness, UPS, and grain size, the relationship obtained by the neural network between the input and output parameters was used in a multi-objective optimization algorithm. The three conflicting objectives in this research were grain size, hardness, and UPS, to be simultaneously optimized with respect to the design variables, namely traverse speed (T), rotational speed (R), and wire diameter (d). This optimization problem can be formulated as follows:

$$\begin{cases} \max hardness\,(T,R,d) \\ \min grainsize\,(T,R,d) \\ \max UPS\,(T,R,d) \\ 6 \leq d \leq 8 \\ 300 \leq R \leq 800 \\ 25 \leq T \leq 40 \end{cases} \qquad (9)$$

The corresponding Pareto front of three objectives, grain size, hardness, and UPS, has been shown in Fig. 20. It is necessary to mention that there is a single set of individuals due to the three-objective optimization illustrated in different planes of the objective functions. Thus, there are some points in each plane that may dominate others in the same plane. However, these
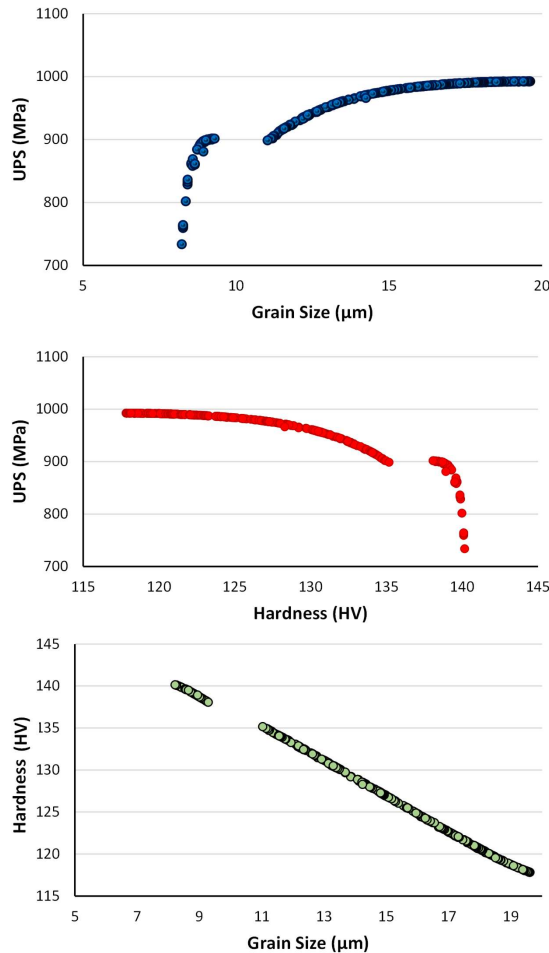
Fig. 20. Optimization result (Pareto front).

individuals are all non-dominated when considering all three objectives simultaneously. According to the Pareto sets, choosing the design variables (traverse speed and rotational speed, and wire diameter) results in the best possible combination of those three objectives.

As can be seen, the answers obtained by multi-objective optimization were a set of nondominated answers. Since only one optimal parameter is needed to produce the product in manufacturing processes, it is necessary to introduce one of the Pareto optimal solutions as the optimal solution. In order to select an optimal parameter from Pareto solutions based on the desired criteria, the TOPSIS method has been used.

In the TOPSIS method, first, the positive ideal solution (S+) and the negative ideal solution (S-) are defined, and then, among the Pareto points, the closest answer to the positive ideal solution and the farthest answer from the negative ideal solution are introduced as the best compromise solution. The TOPSIS method for selecting the best compromise solution is as follows:

1. Enter a matrix for evaluation

2. Normalize the evaluation matrix using the following equation:

$$\tilde{s}_{ij} = \frac{s_{ij}}{\sqrt{\sum_{i=1}^{m} s_{ij}^2}} \tag{10}$$

where $\tilde{s}_{ij}$ is the normalized rating; s_{ij} is the jth objective value of the ith alternative, and m is the number of optimum values.

3. Calculate the weighted evaluation matrix by determining the weight (W) of each objective according to its importance:

$$\sum w_j = 1 \tag{11}$$

$$\hat{s} = w_j \times \tilde{s}_{ij} \tag{12}$$

4. Calculate the positive and negative ideal solution according to the following equations:

$$S^+ = \{(\max \hat{s_{ij}} \,|j \in J_1), (\min \hat{s_{ij}} \,|j \in J_2) \\ , i = 1,2, \dots, n\} \tag{13}$$

$$S^- = \{(\min \hat{s_{ij}} \,|j \in J_1), (\max \hat{s_{ij}} \,|j \in J_2) \\ , i = 1,2, \dots, n\} \tag{14}$$

where J_1 is a set of benefit attributes and J_2 is a set of cost attributes.

5. Using the positive and negative ideal solutions, determine the best (D+) and the worst (D−) alternatives as follows:

$$D_i^+ = \sqrt{\sum_j (\hat{s_{ij}} - s_j^+)^2} \tag{15}$$

$$D_i^- = \sqrt{\sum_j (\hat{s_{ij}} - s_j^-)^2} \tag{16}$$

6. Calculated relative closeness D_i for each Pareto front point as follows:

$$D_i = \frac{D^-}{D^- + D^+} \tag{17}$$

7. Select the best compromise solution whose relative closeness (D_i) is closest to 1.

In order to find the best compromise answer by the TOPSIS, it is necessary to determine the weight of each objective based on its importance. Since the UPS is more critical than the hardness and grain size, the weight given to the UPS is considered more than the other two parameters. For this purpose, a weight of 0.2 was considered for grain size and hardness and a weight of 0.6 for UPS. In this experiment under W = (0.2,0.2,0.6), the best compromise solution has a traverse speed of 36.35 mm/min, a rotational speed of 456 rpm, and a wire diameter of 6 mm.

5. Conclusion

In the present study, the friction stir back extrusion is employed to produce brass wires from its chips. Then the effect of process input parameters such as traverse speed, rotational speed, and wire diameter on the mechanical and microstructural properties of the produced wires was investigated. Numerical methods were used to investigate the temperature history of materials during the process. Finally, the process parameters were obtained using a hybrid optimization method. The results show that

- Lower temperature and higher strain on the surface of the wires reduce the grain size in this area compared to the center of the wire.
- The maximum temperature is reached under the tool shoulder, where the most force and speed of the tool is found.
- The grain size increases in the wires by increasing the rotational speed or decreasing the traverse speed.
- The defect that emerged at the center of the produced sample with 40 mm/min traverse speed reveals that inadequate heat generation at high traverse speed.
- The neural network was able to determine the relationship between inputs and outputs.
- The rotational speed of the tool has the most significant effect on determining the grain size

as well as the hardness.

- Unlike grain size and hardness, the predominant parameter in determining the UPS value of wires is traverse speed.
- Hybrid multi-objective optimization introduced a traverse speed of 36.35 mm/min, a rotational speed of 456 rpm, and wire diameter of 6 mm as optimal parameters.

6. References

[1] A. Heidarzadeh, Tensile behavior, microstructure, and substructure of the friction stir welded 70/30 brass joints: RSM, EBSD, and TEM study, *Archives of Civil and Mechanical Engineering*, 19(1) (2019) 137-146.

[2] A. Heidarzadeh, H.M. Laleh, H. Gerami, P. Hosseinpour, M.J. Shabestari, R. Bahari, The origin of different microstructural and strengthening mechanisms of copper and brass in their dissimilar friction stir welded joint, *Materials Science and Engineering: A*, 735 (2018) 336-342.

[3] A. Heidarzadeh, R.V. Barenji, V. Khalili, G. Güleryüz, Optimizing the friction stir welding of the α/β brass plates to obtain the highest strength and elongation, *Vacuum*, 159 (2019) 152-160.

[4] M. Galai, J. Ouassir, M. Ebn Touhami, H. Nassali, H. Benqlilou, T. Belhaj, K. Berrami, I. Mansouri, B. Oauki, α-Brass and (α+β) brass degradation processes in azrou soil medium used in plumbing devices, *Journal of Bio- and Tribo-Corrosion*, 3(3) (2017) 30.

[5] M.P. Alam, A.N. Sinha, Fabrication of third generation Al–Li alloy by friction stir welding: a review, *Sādhanā*, 44(6) (2019) 153.

[6] O.M. Jarrah, M.A. Nazzal, B.M. Darras, Numerical modeling and experiments of Friction Stir Back Extrusion of seamless tubes, *CIRP Journal of Manufacturing Science and Technology*, 31 (2020) 165-177.

[7] M. Saad, O. Jarrah, M. Nazzal, B. Darras, H. Kishawy, Sustainability-based evaluation of friction stir back extrusion of seamless tubular shapes, *Journal of Cleaner Production*, 267 (2020) 121972.

[8] G. Jamali, S. Nourouzi, R. Jamaati, FSBE process: A technique for fabrication of aluminum wire with randomly oriented fine grains, *Materials Letters*, 241 (2019) 68-71.

[9] M. Shojaeefard, M. Akbari, P. Asadi, Multi objective optimization of friction stir welding parameters using FEM and neural network, *International journal of*

precision engineering and manufacturing, 15(11) (2014) 2351-2356.

[10] M. Akbari, M.H. Shojaeefard, P. Asadi, A. Khalkhali, Hybrid multi-objective optimization of microstructural and mechanical properties of B4C/A356 composites fabricated by FSP using TOPSIS and modified NSGA-II, *Transactions of Nonferrous Metals Society of China*, 27(11) (2017) 2317-2333.

[11] M.H. Shojaeefard, R.A. Behnagh, M. Akbari, M.K.B. Givi, F. Farhani, Modelling and Pareto optimization of mechanical properties of friction stir welded AA7075/AA5083 butt joints using neural network and particle swarm algorithm, *Materials & Design*, 44 (2013) 190-198.

[12] P. Asadi, M. Akbari, H. Karimi-Nemch, 12 - Simulation of friction stir welding and processing, in: M.K.B. Givi, P. Asadi (Eds.), Advances in Friction-Stir Welding and Processing, Woodhead Publishing, 2014, pp. 499-542.

[13] M.H. Shojaeefard, M. Akbari, A. Khalkhali, P. Asadi, Effect of tool pin profile on distribution of reinforcement particles during friction stir processing of B4C/aluminum composites, *Proceedings of the Institution of Mechanical Engineers, Part L: Journal of Materials Design and Applications,* 232(8) (2018) 637-651.

[14] S. Tutunchilar, M. Haghpanahi, M.K. Besharati Givi, P. Asadi, P. Bahemmat, Simulation of material flow in friction stir processing of a cast Al–Si alloy, *Materials & Design*, 40 (2012) 415-426.

[15] I. Dinaharan, S. Zhang, G. Chen, Q. Shi, Titanium particulate reinforced AZ31 magnesium matrix composites with improved ductility prepared using friction stir processing, M*aterials Science and Engineering: A*, 772 (2020) 138793.

[16] M. Akbari, A. Khalkhali, S.M.E. Keshavarz, E. Sarikhani, Investigation of the effect of friction stir processing parameters on temperature and forces of Al–Si aluminum alloys, *Proceedings of the Institution of Mechanical Engineers, Part L: Journal of Materials: Design and Applications* 232(3) (2018) 213-229.

[17] P. Zolghadr, M. Akbari, P. Asadi, Formation of thermo-mechanically affected zone in friction stir welding, *Materials Research Express*, 6(8) (2019) 086558.

[18] L. Wang, Z. Zhang, H. Zhang, H. Wang, K.S. Shin, The dynamic recrystallization and mechanical property responses during hot screw rolling on pre-aged ZM61 magnesium alloys, *Materials Science and Engineering: A*, 798 (2020) 140126.

[19] Z. Zhang, D. Liu, Y. Wang, Y. Pang, F. Zhang, Y. Yang, J. Wang, A novel method for preparing bulk ultrafine-grained material: Three dimensional severe plastic deformation, *Materials Letters*, 276 (2020) 128209.

[20] Q. Wang, Z. Liu, B. Wang, Q. Song, Y. Wan, Evolutions of grain size and micro-hardness during chip formation and machined surface generation for Ti-6Al-4V in high-speed machining, *The International Journal of Advanced Manufacturing Technology*, 82(9) (2016) 1725-1736.

[21] A. Rahimzadeh Ilkhichi, R. Soufi, G. Hussain, R. Vatankhah Barenji, A. Heidarzadeh, Establishing mathematical models to predict grain size and hardness of the friction stir-welded AA 7020 aluminum alloy joints, *Metallurgical and Materials Transactions B*, 46(1) (2015) 357-365.

[22] M. Akbari, P. Asadi, M.K. Besharati Givi, G. Khodabandehlouie, 13 - Artificial neural network and optimization, in: M.K.B. Givi, P. Asadi (Eds.), Advances in Friction-Stir Welding and Processing, Woodhead Publishing, 2014, pp. 543-599.

[23] Y.C. Du, A. Stephanus, Levenberg-Marquardt neural network algorithm for degree of arteriovenous fistula stenosis classification using a dual optical photoplethysmography sensor, *Sensors*, 18(7) (2018) 2322.

[24] P. Asadi, M. Akbari, M.K. Besharati Givi, M. Shariat Panahi, Optimization of AZ91 friction stir welding parameters using Taguchi method, *Proceedings of the Institution of Mechanical Engineers, Part L: Journal of Materials Design and Applications,* 230(1) (2016) 291-302.